Appl. Phys. B 74 [Suppl.], S133–S144 (2002)
DOI: 10.1007/s00340-002-0911-y

Applied Physics B
Lasers and Optics

T. BRIXNER
G. KRAMPERT
P. NIKLAUS
G. GERBER✉

Generation and characterization of polarization-shaped femtosecond laser pulses

Physikalisches Institut, Universität Würzburg, Am Hubland, 97074 Würzburg, Germany

Received: 2 October 2001 / Revised version: 12 November 2001
Published online: 5 July 2002 •

ABSTRACT We demonstrate the generation and complete characterization of femtosecond laser pulses which change their intensity, frequency, and light polarization almost arbitrarily within a single pulse employing the new technique of femtosecond polarization pulse shaping. Specifically, the degree of polarization ellipticity as well as the orientation of the elliptical principal axes can be varied as a function of time in a completely controllable manner, using a 128-pixel, two-layer, liquid-crystal display (LCD) inside a zero-dispersion compressor. A mathematical formalism is presented with which polarization-shaped pulse parameters can be calculated and used to generate intuitive quasi-three-dimensional electric field representations. However, laboratory realization requires accurate and complete experimental pulse characterization methods. For this purpose, the technique of dual-channel spectral interferometry is employed. Furthermore, Jones calculus for polarization-shaped pulses with experimentally determined Jones matrices is developed. It can be used to predict and account for all pulse-shape modifications occurring in various optical elements of the pulse shaper and the experimental setup.

PACS 42.65.Re; 42.79.Hp; 42.60.-v

1 Introduction

Femtosecond laser pulse shaping has become a very powerful and versatile tool in the last few years. The main idea of so-called "Fourier-domain pulse shaping" is to disperse the inherently broad femtosecond pulse spectrum spatially, thereby allowing for convenient manipulation of the spectral intensity and/or phase. After recollimation, specifically tailored temporal shapes are created. Initial experiments on picosecond [1] and femtosecond [2] shaping were done with fixed-shape amplitude or phase masks. Subsequent development of high-quality liquid-crystal display (LCD) spatial light modulators (SLM) opened the possibility for rapid and reliable phase manipulation [3, 4]. The introduction of two-layer sandwiched LCDs has made feasible independent phase and amplitude control [5]. Acousto-optic modulators [6, 7] as well as deformable mirrors [8] have also been reported as shaping devices. The whole field of femtosecond laser pulse shaping has been reviewed recently [9].

The prospect to generate arbitrarily shaped temporal electric field profiles on a femtosecond time scale has triggered significant developments in many fields of fundamental and applied research, such as ultrashort laser technology [10–13], telecommunications [14], and especially quantum control [15, 16]. In the latter area, specifically shaped pulses have been used to control fluorescence yields in dye molecules [17], to control the yield of molecular photodissociation reactions [18], to control atomic two-photon transitions [19, 20], to tailor atomic wave functions [21], to excite selective molecular vibrations [22], to control vibrational dynamics [23, 24] as well as ultrafast semiconductor nonlinearities [25], and to increase the efficiency of high-harmonic generation [26].

All these successful experiments were made possible by altering the amplitude and phase of the electric field as a function of time. However, the electric field is a vectorial quantity. The range of possible applications could be expected to increase dramatically if it were possible to also alter the polarization state of light as a function of time. For example, polarization-shaped femtosecond light pulses have been suggested for the generation [27, 28] and characterization [29] of attosecond light pulses, as well as for optical control of lattice vibrations [30]. Another "hot-topic" application could be the selective production of chemical enantiomers [31–36], for which specific temporal polarization profiles should play an important role. In any event, light pulses where the electric field vector oscillates in an additional dimension offer extensive experimental possibilities, since most investigated physical systems are three-dimensional themselves.

In principle, the generation of time-dependent polarization profiles can be achieved by splitting the electric field into orthogonal polarization components within a Mach–Zehnder interferometer. Each of the two arms can then be manipulated separately. In the case of broadband light sources, the application of frequency-dependent phase modulation leads to a time-varying polarization state after recombination of the two components. However, up to now only simple polarization profiles have been produced in such configurations using fixed-shape phase modifications [37–40]. These methods do not offer any flexibility. Only a very limited number of dif-

✉ Fax: +49-931/888-4906, E-mail: gerber@physik.uni-wuerzburg.de

ferent pulse shapes can be generated, and changing the pulse shape requires mechanical reconstruction and new alignment of the experimental setup. The use of femtosecond pulse shapers in each of the interferometric arms separately has been suggested [39], but not experimentally carried out.

In any case, a serious difficulty with all these interferometric techniques is the requirement of optical stability. If the relative optical path length between the two arms fluctuates by only a small fraction of the optical wavelength, the resulting polarization state already changes dramatically. It is experimentally very difficult to ensure phase stability, and hence reproducible conditions, over a long time period. The stability issues can be solved if the polarization components are not spatially separated at all, but rather travel along an identical beam path as for example in wave plates. However, instead of using fixed optical crystals, LCDs offer much more flexibility. Manipulation of the polarization state of continuous-wave light, but not as a function of time or frequency, was demonstrated by use of a single-pixel three-layer LCD [41]. In an extension to that technique, many-pixel LCDs were used to generate continuous-wave light fields where the polarization state varied along the transverse beam profile [42]. It was also shown that many-pixel two-layer LCDs can in principle be used to shape two independent spectrally resolved polarization components [5]. In that experiment, however, due to the very low diffraction efficiency of the gratings for p-polarization, the intensity of the p-component was smaller than the s-component's by a factor of about 120, thereby effectively only producing amplitude-modulated light pulses, not polarization-modulated pulses.

We have recently introduced the technique of computer-controlled femtosecond polarization pulse shaping [43] where the light's polarization state reaches different linear and elliptical orientations with varying degrees of ellipticity within a single laser pulse, while the two independent and temporally interfering polarization components reach equal intensity levels. In this contribution, we describe in detail the experimental realization of the pulse-shaper-setup (Sect. 2) and the mathematical representation of the laser pulses (Sect. 3). A formalism for the transformation from linear to elliptical pulse parameters is introduced (Sect. 3.1). These parameters describe the temporal evolution of the electric field of these complex polarization-shaped laser pulses, and an intuitive quasi-three-dimensional representation can be generated (Sect. 3.2). Complete experimental characterization is described in Sect. 4. For this purpose, dual-channel spectral interferometry is employed (Sect. 4.1). Furthermore, as optical elements in the experimental setup can induce modifications of the polarization-state (Sect. 4.2), an alternative pulse characterization method by Jones calculus is described, which takes these effects into account (Sect. 4.3). Jones analysis and dual-channel spectral interferometry are shown to deliver equivalent results in Sect. 4.4. Thus complex polarization-shaped pulses can be generated and analyzed experimentally (Sect. 4.5). Finally, the paper is concluded in Sect. 5.

2 Experimental setup

The femtosecond polarization pulse-shaper setup [43] is shown in Fig. 1. It consists of an all-reflective zero-dispersion compressor in a $4f$-geometry. The input light, polarized along the x axis, is diffracted by a holographic grating (1800 lines/mm) in Littrow configuration, tilted upwards by a small angle. The spatially dispersed spectrum hits a concave cylindrical mirror, placed at a distance of one focal length (80 mm) from the grating. A folding mirror (minimizing lens aberrations as compared to "direct" beam geometries) directs the spectrum along the x-axis of a two-layer LCD (Cambridge Research & Instrumentation), which is placed in the so-called Fourier plane of the zero-dispersion compressor, at a distance of another focal length from the first cylindrical mirror. Each layer consists of 128 separate pixels, sized 100 μm width by 2 mm height. The z axis defines the direction of propagation, and the preferential orientation axes of the nematic liquid-crystal molecules in the first and in the second LCD layers are located in the x–y plane, rotated by $-45°$ and $+45°$, respectively, from the x axis. The x-polarized input light has polarization components of equal magnitude along these two orientation axes, labeled as 1 and 2 in the following discussion. If suitable voltages are applied to the separate pixels, the liquid-crystal molecules are tilted in the 1–z and 2–z planes, respectively, thereby permitting independent changes of the refractive indices for the two corresponding light-polarization components at 128 individual frequency intervals throughout the laser spectrum.

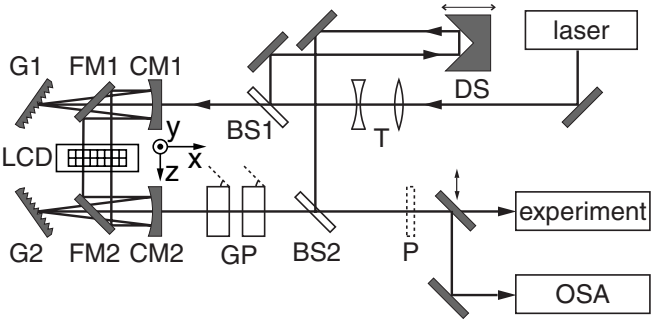

FIGURE 1 Setup of the polarization pulse shaper. A telescope (T) is used to adjust the beam diameter of the Ti:sapphire femtosecond laser (800 nm, 80 fs, 1 mJ, 1 kHz). Beam splitters (BS1 + BS2) and a delay stage (DS) provide an unshaped reference beam for the pulse characterization, which is carried out in the beam path toward the experiment. For that purpose a polarizer (P) can be introduced in the beam path. The pulse shaper itself consists of an all-reflective zero-dispersion compressor employing holographic gratings (G1 and G2), cylindrical mirrors (CM1 and CM2), planar folding mirrors (FM1 and FM2), and a double-layer liquid-crystal display (LCD). All the mirrors have "protected silver" coating. Compensation for the polarization-sensitive grating diffraction efficiency is achieved by transmitting the beam through a stack of glass plates (GP) at approximately Brewster's angle

Recollimation of the laser beam is achieved by the symmetrically arranged second set of folding mirror, concave mirror, and grating. The grating efficiency is approximately 90% (30%) for x-(y-)polarized light. To compensate for this difference, a stack of four glass plates at approximately Brewster's angle is used at the output of the pulse shaper, reflecting 30% of the x-component out of the beam path and transmitting 100% of the y-component. Variations of the total pulse energy for different pulse shapes are smaller than 1%. Since we use cylindrical lenses and a separate telescope in front of the pulse shaper to adjust the beam diameter from ≈ 8 mm down to 2 mm, it is possible to use femtosecond oscillator

as well as amplified laser pulses without the danger of damaging the optical components. Our laser system consists of a home-built Ti:sapphire oscillator and a commercial regenerative amplifier employing chirped-pulse amplification. It is capable of delivering 80-fs, 800-nm, 1-mJ pulses at a 1-kHz repetition rate. The total energy throughput of the polarization pulse shaper (including telescope, pulse characterization pickoffs and Brewster stack) is approximately 15%, such that polarization-shaped laser pulses of 150 μJ energy are available for experiments. Note that the polarization pulse shaper is easily converted into an amplitude-and-phase shaper by simply adding a polarizer after the LCD with its transmissive axis parallel to x, for instance. The "reference" beam line for pulse characterization will be explained in Sect. 4.1.

The calibration of the LCD is performed similar to the technique described in [4, 9]. For a complete calibration of the pulse shaper, two individual measurements are necessary: the calibration of the phase shift as a function of pixel voltage and the assignment of the wavelengths to their corresponding pixel numbers. To calibrate the pixel voltage settings, the pulse shaper is operated in amplitude modulation mode by employing crossed polarizers before and after the LCD, respectively. The calibration is then performed for each of the two layers of the LCD separately. The transmitted intensity of the Ti:sapphire laser through an arbitrary pixel is recorded with a spectrometer (such that the neighboring pixels in different wavelength regions do not interfere) as a function LCD pixel voltage U. The phase shift $\Delta\Phi(U)$ is then connected to the transmission $T(U)$ by

$$\Delta\Phi(U) = \arccos(1 - 2T(U)). \tag{1}$$

The voltage-dependent optical path length difference $\Delta l_{\mathrm{opt}}(U)$ can then be calculated by

$$\Delta l_{\mathrm{opt}}(U) = \frac{\Delta\Phi(U)}{2\pi}\lambda = [n(U) - n(0)]l \tag{2}$$

separately for each layer. This conversion takes the wavelength dependence of $\Delta\Phi(U)$ into account, so that the same calibration $\Delta l_{\mathrm{opt}}(U)$ can be used for all LCD pixels across the laser spectrum. For the calibration of the pixel number versus wavelength, the pulse shaper is run again in amplitude modulation mode. Alternating pixels are now set to maximum and minimum transmission, respectively, and the modulated spectrum of the Ti:sapphire laser is recorded. By counting the minima and maxima in the modulated spectrum, the pixel numbers can be attributed to their corresponding wavelength. Additionally, for an unambiguous assignment, one pixel in the middle of the LCD is set to a transmission of 50% to distinguish it from the other pixels at minimum or maximum transmission. The nonlinear calibration curve can then be obtained by fitting these data points.

The principle of operation of the polarization pulse shaper is illustrated for one particular frequency component in Fig. 2. Starting with the projection of the x polarization (left side) onto the two components 1 and 2 (dashed lines), the propagation through the LCD starts with identical phase. However, the tensorial nature of the susceptibility tensor is responsible for direction-dependent refractive indices, and thus for a difference in optical wavelength between components 1 (dark gray) and 2 (light gray). These wavelengths can be varied individually by applying suitable voltages to the electrodes of the corresponding LCD layers. The momentary electric field vector resulting at the exit plane of the LCD (arrow on the right) is constructed geometrically by appropriate projections of the phase-shifted components 1 and 2 (dashed lines). However, since light is a travelling wave, the momentary phases are functions of time, and the tip of the electric field vector evolves along the ellipse shown on the right side of the diagram. The degree of ellipticity depends on the relative phase difference between components 1 and 2, acquired upon propagation through both LCD layers. Since the electric field amplitudes along the axes 1 and 2 remain constant upon transmission, any possible elliptical polarization has to be tangential to a square as indicated in the figure with its sides parallel to the 1 and 2 directions. Thus, the principal axes of any polarization ellipse of one particular frequency component point always along the x and y directions. However, such transformations from linearly to elliptically polarized light can be performed independently for each spectral component. The total electric field in the time domain then depends on the interference between all the individual elliptically polarized frequency components. This leads to complex polarization-modulated laser pulses in which there is no restriction on the direction of the principal axes.

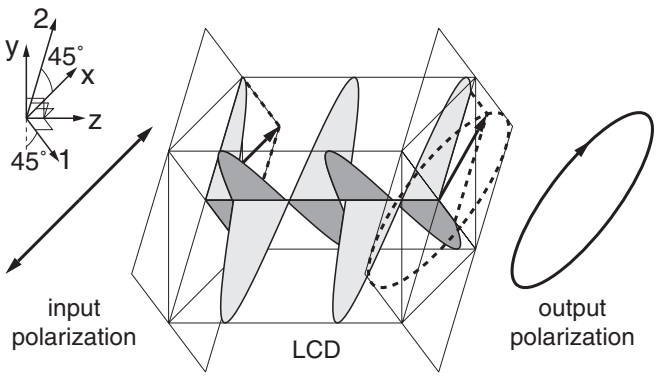

FIGURE 2 Principle of operation of the polarization pulse shaper. The linearly x-polarized input light of one particular frequency component can be decomposed into the polarization components 1 (*dark gray*) and 2 (*light gray*), which propagate collinearly but with different optical wavelengths. The resulting phase difference after passage through the LCD – which can be varied by applying suitable voltages – leads to elliptically polarized output light

3 Description of polarization-shaped laser pulses

In this section, a mathematical formalism for the description and representation of complex polarization-shaped femtosecond laser pulses is developed by transforming linear into elliptical pulse parameters (Sect. 3.1) and illustrated by means of an example (Sect. 3.2).

3.1 *Elliptical pulse parameters*

Since light is a transverse electromagnetic wave, two linearly independent vector components of the electric field at each point in space are sufficient for a complete de-

scription. The electric field is then written as

$$\boldsymbol{E} = \begin{pmatrix} E_1 \\ E_2 \end{pmatrix}, \tag{3}$$

where E_1 and E_2 are given in either frequency or time domain. It is convenient (although not necessary) to choose the basis vectors linear and parallel to the LCD orientation axes 1 and 2. Assume that the vectorial electric field profile is given by its spectral components $E_1(\omega)$ and $E_2(\omega)$. The temporal electric field components $E_1(t)$ and $E_2(t)$ can then be obtained from $E_1(\omega)$ and $E_2(\omega)$ by inverse Fourier transformations. Polarization-shaped laser pulses can thus be described by

$$\begin{pmatrix} E_1(t) \\ E_2(t) \end{pmatrix} = \begin{pmatrix} A_1(t)\cos[\omega_0 t + \varphi_1(t)] \\ A_2(t)\cos[\omega_0 t + \varphi_2(t)] \end{pmatrix} \tag{4}$$

in terms of temporal amplitudes $A_1(t)$ and $A_2(t)$, the center frequency ω_0, and temporal phase modulations $\varphi_1(t)$ and $\varphi_2(t)$. Mathematically, this "linear representation" already contains the complete information about the scalar and the vectorial properties of the electric field. However, the two components $E_1(t)$ and $E_2(t)$ interfere coherently, and the momentary polarization state is not easily extracted directly from (4). Therefore a more intuitive "elliptical representation" is developed in the following. For the sake of simplicity, the time arguments are omitted throughout the discussion.

In the slowly-varying envelope approximation, the time evolution of the electric field vector within one oscillation period around time t is given by an ellipse (Fig. 3). The principal axes $\tilde{A}_1$ and $\tilde{A}_2$ are in general different from the laboratory-frame amplitudes A_1 and A_2, but they can be obtained by a principal-axis transformation. This leads to a determination of the angle of ellipticity ε where

$$\tan\varepsilon = \tilde{A}_2/\tilde{A}_1. \tag{5}$$

The angle of the ellipse's orientation θ is given by the angle between the major elliptical principal axis $\tilde{A}_1$ and the laboratory-frame A_1 axis. To calculate ε and θ, the following "auxiliary" angles are defined:

$$\chi = \arctan\frac{A_2}{A_1} \quad \in [0, \pi/2], \tag{6}$$

which describes the ratio of the two laboratory-frame temporal amplitude components, and

$$\delta = \varphi_2 - \varphi_1 \quad \in [-\pi, \pi], \tag{7}$$

which describes the difference between the corresponding temporal phase modulations. In these and the following equations, it is important to note the definition intervals as indicated by square brackets. It can be shown that

$$\theta = \begin{cases} \tilde{\theta} & \in \left[-\pi/4, \pi/4\right] \quad \text{if } \chi \le \pi/4, \\ \tilde{\theta} + \pi/2 & \in \left[\pi/4, \pi/2\right] \quad \text{if } \chi > \pi/4 \wedge \tilde{\theta} < 0, \\ \tilde{\theta} - \pi/2 & \in \left[-\pi/2, -\pi/4\right] \quad \text{if } \chi > \pi/4 \wedge \tilde{\theta} \ge 0, \end{cases} \tag{8}$$

where

$$\tilde{\theta} = \frac{1}{2}\arctan\left[\tan(2\chi)\cos\delta\right] \quad \in \left[-\pi/4, \pi/4\right]. \tag{9}$$

Furthermore, it can be shown that

$$\varepsilon = \frac{1}{2}\arcsin\left[\sin(2\chi)\sin\delta\right] \quad \in \left[-\pi/4, \pi/4\right]. \tag{10}$$

With these relations, the momentary "shape" and "orientation" of the ellipse (i.e. the polarization state) are determined. The conventions are such that the orientation angle θ of the major principal axis is defined in the first or fourth quadrant (not in the second or third), i.e. $\theta \in [-\pi/2, \pi/2]$. The angle of ellipticity is always defined in terms of the ratio of the minor divided by the major principal axis, i.e. $|\varepsilon| \le \pi/4$. The sign of ε is used to distinguish the helicity, i.e. the sense of rotation of the electric field vector. Positive values of ε correspond to a momentarily left, negative values of ε to a momentarily right elliptically polarized light state. The convention here is such that the helicity is determined by monitoring the evolution of the electric field vector as a function of time in a plane normal to the direction of propagation, and viewing this plane along the negative z direction (opposite to the direction of pulse propagation). The momentary "size" of the electric field ellipse depends upon the total intensity

$$I = I_1 + I_2 = \tilde{I}_1 + \tilde{I}_2, \tag{11}$$

where the individual intensity components are proportional to the squares of the corresponding amplitudes. The second equality in (11) is due to the fact that the total pulse energy – and hence the total intensity – is independent of the chosen coordinate system.

The last elliptical pulse characterization parameter is called "total phase" $\varphi(t)$, which we have suggested to be used as the last of the required four independent pulse characterization parameters [43]. Just as $\varepsilon(t)$ and $I(t)$, $\varphi(t)$ will be defined in such a way that its value does not depend upon the choice of the coordinate system (whereas $\theta(t)$ describes the orientation of the ellipse with respect to the laboratory reference frame). For a motivation of its definition, consider first the linearly polarized light component $E_1(t) = A_1(t)\cos[\omega_0 t + \varphi_1(t)]$ alone.

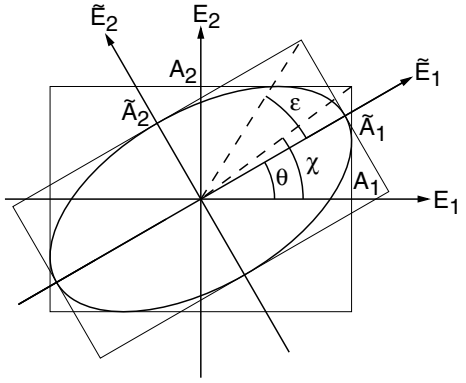

FIGURE 3 Elliptical pulse parameters. The light polarization ellipse is characterized by the major principal axis $\tilde{A}_1$ and the minor principal axis $\tilde{A}_2$. These two amplitudes define the angle of ellipticity ε. The ellipse-inherent $\tilde{E}_1$–$\tilde{E}_2$ coordinate system is rotated by the orientation angle θ with respect to the laboratory-frame E_1–E_2 coordinate system. In the laboratory system, the ratio of the amplitude components A_1 and A_2 defines the angle χ as indicated

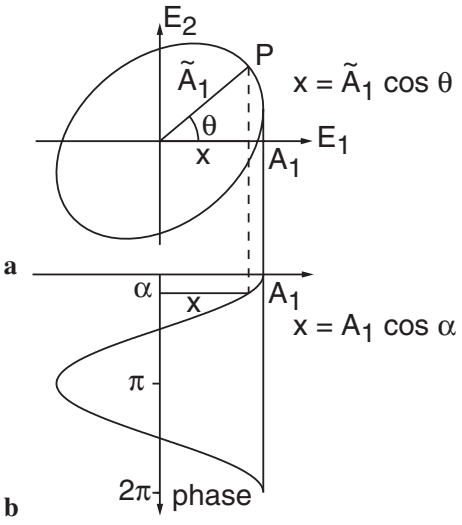

FIGURE 4 Determination of total phase. This figure illustrates the connection between **a** the electric field oscillation of polarization-shaped light pulses and **b** the projection of the oscillation onto one polarization component. The position of the perihelion (P) of the light ellipse at orientation angle θ is related to the "geometrical" phase α of the associated oscillation of component E_1. This relation can be evaluated by equating the "distances" x from both parts of this figure

Here the phase $\omega_0 t + \varphi_1(t)$ covers the interval $[0, 2\pi]$ within one oscillation of the electric field as illustrated in Fig. 4b. The reference point of zero phase is always passed when the electric field has reached its amplitude $E_1(t) = A_1(t)$. For polarization-shaped light, the phase reference point is therefore set by analogy at the perihelion P (Fig. 4a) of the momentary light ellipse, i.e. at that point in the first or fourth quadrant where the total electric field has reached its amplitude given by the major principal axis $\tilde{A}_1(t)$. This definition of $\varphi(t)$ has the appealing consequence that in temporal pulse intervals for which one polarization component is small (e.g. $A_1(t) \approx 0$), the total phase resembles the phase of the remaining component (i.e. $\varphi(t) \approx \varphi_2(t)$). The total phase modulation $\varphi(t)$ then arises as a combination of two effects: the phase modulation $\varphi_1(t)$ associated with component $E_1(t)$, and the "geometrically" determined phase $\alpha(t)$ associated with that fraction of one light oscillation which takes the electric field vector from pointing along the laboratory-frame A_1 component to pointing along the ellipse-inherent $\tilde{A}_1$ principal axis (see Fig. 4). For a correct description it is necessary to take into account if the momentary perihelion lies in the first quadrant ($\theta \geq 0$) or in the fourth quadrant ($\theta < 0$), and if the light field oscillates counter-clockwise ($\varepsilon \geq 0$) or clockwise ($\varepsilon < 0$). The total phase is then defined as

$$\varphi = \begin{cases} \varphi_1 + \alpha & \text{if } (\varepsilon \geq 0 \wedge \theta \geq 0) \vee (\varepsilon < 0 \wedge \theta < 0), \\ \varphi_1 - \alpha & \text{otherwise.} \end{cases} \tag{12}$$

According to Fig. 4, the geometrical phase α is determined by equating the length x from Fig. 4a and b such that

$$A_1 \cos\alpha = \tilde{A}_1 \cos\theta. \tag{13}$$

Using (5) and (11), this leads to

$$\varphi = \varphi_1 + \operatorname{sign}\{\theta\varepsilon\} \arccos\left[\sqrt{\frac{I}{I_1}} \cos\theta \cos\varepsilon\right]. \tag{14}$$

Because of the application of the arccosine function within (14), "phase jumps" of $\pm\pi$ have to be removed afterwards if $\varphi(t)$ is desired as a continuous function of time. The temporal derivative of the total phase can be used to calculate the momentary frequency

$$\omega(t) = \omega_0 + \frac{\mathrm{d}\varphi(t)}{\mathrm{d}t}. \tag{15}$$

In other words, the oscillation period T around time t of the electric field between two successive passes of the perihelion is

$$T = \frac{2\pi}{\omega(t)} = \frac{2\pi}{\omega_0 + \mathrm{d}\varphi(t)/\mathrm{d}t}. \tag{16}$$

3.2 *Example*

At this point, it is helpful to discuss a first example of a polarization-shaped laser pulse. Three mathematically equivalent representations are shown in this simulation (Fig. 5), employing frequency-domain linear parameters $\{I_1(\omega), I_2(\omega), \Phi_1(\omega), \Phi_2(\omega)\}$ in Fig. 5a, time-domain linear parameters $\{I_1(t), I_2(t), \varphi_1(t), \varphi_2(t)\}$ in Fig. 5b, and time-domain elliptical parameters $\{I(t), \varphi(t), \theta(t), \varepsilon(t)\}$ in Fig. 5c. A Gaussian-shaped laser spectrum is assumed (Fig. 5a, top part) which supports bandwidth-limited laser pulses of 80 fs duration. In an ideal polarization pulse shaper, the x-polarized input intensity is split equally into the two polarization components $I_1(\omega)$ and $I_2(\omega)$, and the double-layer LCD can be used to directly apply spectral phase modulations (Fig. 5a, bottom part): a quadratic phase of $b_2 = 1 \times 10^4$ fs^2 to $\Phi_1(\omega)$ (dashed line), and a linear phase of $b_1 = -200$ fs to $\Phi_2(\omega)$ (solid line), with the spectral phase coefficients of nth order defined as $b_n = \mathrm{d}^n\Phi(\omega)/\mathrm{d}\omega^n|_{\omega=\omega_0}$. In general, the coefficient of zeroth-order describes a constant phase and the coefficient of first-order a temporal translation of the laser pulse. The coefficients of higher order are responsible for changes in the temporal structure of the electric field.

As can be seen in Fig. 5b (top part), the employed spectral phase modulations lead to changes in the temporal pulse envelopes. The $I_1(t)$ component (dashed line) is temporally broadened, while the $I_2(t)$ component (solid line) is simply temporally translated by -200-fs and still satisfies the minimum time–bandwidth product. These observations are confirmed by the temporal phase analysis (Fig. 5b, bottom part). Component $\varphi_1(t)$ (dashed line) is given by a parabola of second order (indicating linear chirp), and component $\varphi_2(t)$ (solid line) is constant (i.e. unchirped) in the regions of nonvanishing intensity $I_2(t)$.

However, the polarization-state evolution is not seen directly in Fig. 5a and b. The elliptical description (Fig. 5c) is appropriate for that purpose. Here, the total intensity $I(t)$ (top part, solid line) reflects the double-pulse structure of the individual components $I_1(t)$ and $I_2(t)$. The total phase $\varphi(t)$ (top

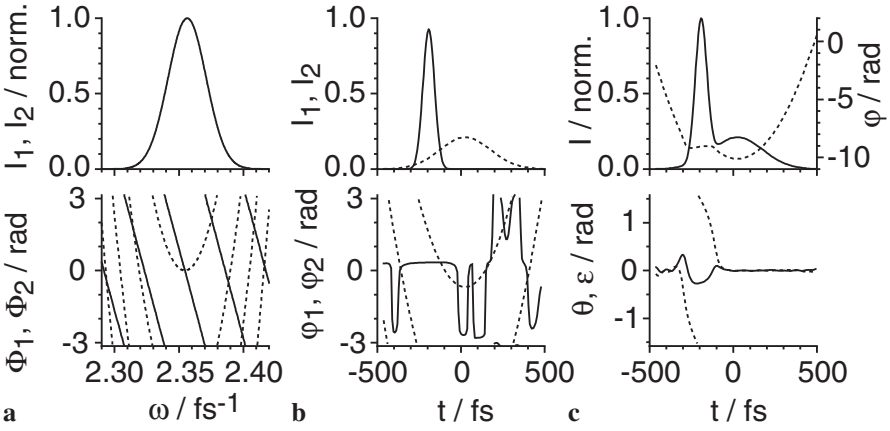

FIGURE 5 Representation of a polarization-shaped laser pulse. This figure shows **a** spectral intensities (*top part*) and spectral phases (*bottom part*) for component E_1 (*dashed line*) and component E_2 (*solid line*), **b** temporal intensities (*top part*) and temporal phase modulations (*bottom part*) for component 1 (*dashed line*) and component 2 (*solid line*), and **c** the temporal total intensity (*top part*, *solid line*) and total phase (*top part*, *dashed line*) as well as the temporal evolution of the ellipticity angle (*bottom part*, *solid line*) and the orientation angle (*bottom part*, *dashed line*)

part, dashed line) is seen to follow the parabolic shape of $\varphi_1(t)$ in the beginning and in the end of the pulse where only component $I_1(t)$ is present, and it follows the linear slope of $\varphi_2(t)$ in that temporal region where $I_2(t)$ dominates. This behavior illustrates the utility of the coordinate-frame-independent definition of the total phase. Apart from the parameters of total intensity and total phase (Fig. 5c, top part), the evolution of the polarization state can be inferred from Fig. 5c (bottom part). In the beginning of the pulse and in its second half, both $\varepsilon(t)$ (solid line) and $\theta(t)$ (dashed line) are approximately zero, indicating vanishing ellipticity (i.e. linear polarization) as well as an orientation along the laboratory-frame coordinate axis A_1, respectively. This is of course consistent with the fact that in those temporal intervals only the component $I_1(t)$ is present (Fig. 5b, top part, dashed line). In the intermediate time regime when both of the components $I_1(t)$ and $I_2(t)$ contribute substantially, interference leads to a change in the polarization state such that $\varepsilon(t)$ as well as $\theta(t)$ deviate from zero.

As the temporal variation of the polarization state within one laser pulse is a substantial feature of the polarization-shaped pulses, it is helpful for the understanding to have an alternative and complete representation available which displays these changes in a single and intuitive graph including the other pulse parameters. The result is a quasi-three-dimensional electric field representation of the polarization-modulated laser pulse (Fig. 6). Temporal snapshots of the polarization-state ellipses from Fig. 3 are stacked along the horizontal spatial coordinate, indicating the vectorial electric field amplitudes at each point in time throughout the laser pulse. Time evolves from left to right, and the lower (upper) shadow represents the electric field amplitude of the 1 (2) component alone. The total phase can be indicated by the corresponding momentary frequency. In a color plot, "green" is used for the center frequency ω_0, "red" tones are used for lower, and "blue" tones for higher oscillation frequencies. It can be seen that the laser pulse in Fig. 6 is linearly polarized along the E_1 axis (displayed horizontally here) in the beginning, followed by a time interval in which additional contributions from the E_2 component interfere (displayed vertically). This leads to elliptically polarized light, along with a rotation of the orientation in accordance with Fig. 5c. The second half of the laser pulse is purely 1-polarized again, and the "ellipses" have no extension in the vertical direction. The derivative of the total phase (Fig. 5c, upper part, dashed line) leads to an upchirp in the beginning and in the second half of the laser pulse (colors evolving from red to blue) and to an unchirped contribution when the E_2 component dominates (constant green color). The amplitude envelope of component E_1 (lower shadow) displays clearly the longer pulse duration introduced by the second-order spectral phase modulation. The evolution of polarization state, intensity, and chirp is thus apparent from a single illustration.

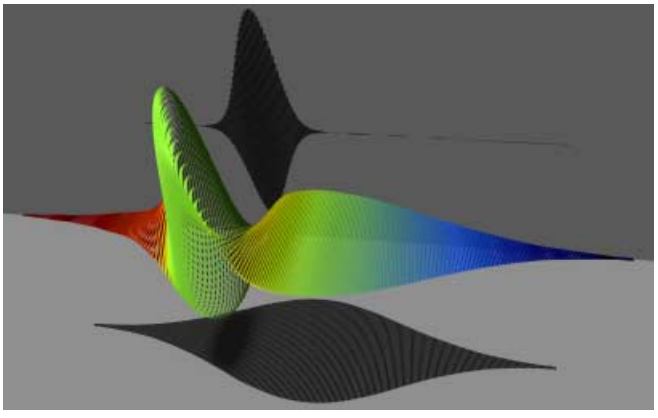

FIGURE 6 Quasi-three-dimensional electric field representation for the laser pulse of Fig. 5. Time evolves from left to right, and electric field amplitudes are indicated by the sizes of the corresponding ellipses. The momentary frequency can be indicated by colors, and the shadows represent the amplitude envelopes of component E_1 (*bottom*) and component E_2 (*top*) separately

4 Characterization of polarization-shaped laser pulses

With the ability to generate almost arbitrarily shaped femtosecond laser pulses, it is necessary to employ suitable experimental pulse characterization methods. Furthermore, there are a number of additional difficulties with polarization-shaped pulse analysis which are not present in the linearly polarized case. One issue mentioned here is the modification of the polarization profile upon interaction with optical elements. It is therefore very important to characterize the pulse shapes directly at the point of the experiment. Therefore, a simple and yet efficient single-shot pulse characterization technique is employed. The pulse-characterization

technique discussed here is dual-channel spectral interferometry (Sect. 4.1). Another possibility for correct and complete characterization is to find a "calibration" which takes into account additional variations induced by the optical elements (Sect. 4.2). As will be shown, such effects can be accounted for by Jones-matrix calculus (Sect. 4.3), which delivers results equivalent to dual-channel spectral interferometry (Sect. 4.4). Complex polarization-shaped laser pulses can thus be generated and experimentally characterized (Sect. 4.5).

4.1 *Dual-channel spectral interferometry*

The use of dual-channel spectral interferometry relies on the technique of single-channel spectral interferometry [44–46], which can be used as a pulse characterization method for linearly polarized light pulses needing only noniterative data evaluation. Furthermore, it employs a purely linear detection scheme and therefore offers high sensitivity. As an important difference to the autocorrelation [47] or the FROG technique [48, 49], the pulse shaper is placed here in one arm of an interferometer rather than in front of the first beam splitter. The resulting electric field after the recombining beam splitter of the interferometer is a superposition of an unshaped reference laser pulse $E_0(t)$ and the shaped pulse $E(t)$ to be analyzed. The two laser pulses are delayed with respect to each other by a time τ which is set at a fixed value such that the two pulses do not overlap temporally. This temporal separation is not varied for the measurement, but it leads to a spectral interference pattern subsequently detected by a spectrometer. The fringes appear at a period of approximately $2\pi/\tau$, but they are modulated according to the phase introduced by the pulse shaper. Quantitative analysis of spectral interferometry data is possible by a Fourier-transform method [46, 50, 51], yielding the relative phase $\Phi(\omega) - \Phi_0(\omega)$ between shaped and reference pulse. The phase $\Phi_0(\omega)$ of the reference laser pulse has to be determined separately. This can be done by FROG, for example, and the combination of the two techniques, also called TADPOLE (temporal analysis by dispersing a pair of light electric-fields) [52], then delivers the complete information about the electric field.

Dual-channel spectral interferometry works similar to the single-channel technique, but it requires the acquisition of six different laser spectra: the reference and shaped beams separately as well as combined for both polarization components. It had already been reported that such a setup could be used to analyze (simple) time-dependent polarization profiles [37, 53]. However, that discussion did not include the issue of total phase $\varphi(t)$. Since the reference pulse is linearly polarized, it can be characterized by standard techniques. For example, the reference pulse can be analyzed by FROG. The combination with dual-channel spectral interferometry has been called POLLIWOG (polarization-labeled interference versus wavelength of only a glint) [37].

The experimental setup for the pulse-characterization technique with dual-channel spectral interferometry is shown in Fig. 1. With the help of a first beam splitter (BS1), a small pick-off from the x-polarized input light is sent over a variable delay stage (DS). The two parts are then recombined collinearly at a second beam splitter (BS2). A polarizing film (P in Fig. 1, Polarcore) is placed directly into the recombined beam with its transmission axis at either $+45°$ or $-45°$ orientation with respect to the x axis. In this way, both polarization components of the recombined laser beam can then be directed separately into the spectrometer by one single set of mirrors. Computer-controlled automatic shutters are used to facilitate the measurement of the interference spectra, as well as the spectra of shaped and reference pulse alone. Spectral interference patterns of both components are recorded by a multichannel optical spectrum analyzer (OSA) with 2048 pixels and a resolution of 0.05 nm.

For determination of the elliptical pulse parameters it is essential to measure the relative phase between the two polarization components in all spectral or temporal regions. For example, the coordinate δ (7) is determined by the momentary value of the temporal phase difference between the two light polarization components. Therefore, it is important here that the relative phase between the two polarization components is always preserved. This relative phase can be determined (modulo 2π, which is sufficient) from the relative phase of the interference fringes between the two components, which are seen when the reference and shaped pulse both hit the spectrometer. This means that the exact positions of the interference maxima and minima of one polarization component with respect to those from the other component are evaluated. The experimental setup has to be stable enough to guarantee that the peak positions do not shift between the interferometric measurement of one and the other polarization component. This is generally feasible because stability is only required over a short time period. It is not critical if the fringe positions shift between successive measurements of different pulse shapes. Alternatively, two separate spectrometers or an imaging spectrometer with spatial resolution (for the two polarization components) could be used. It is emphasized again that the generation of the polarization-shaped pulses does not require interferometric stability, because both polarization components always travel along the same beam path.

In the following experimental example, linear spectral phase modulation of $b_1 = 500\,\mathrm{fs}$ was applied to polarization component 1, and quadratic phase modulation of $b_2 = 5 \times 10^3\,\mathrm{fs}^2$ was applied to component 2. The six collected laser spectra necessary for the analysis are shown in Fig. 7. The two components of the reference beam (Fig. 7a and d) display the smooth Gaussian envelope of the Ti:sapphire oscillator used here. In contrast, the shaped spectra (Fig. 7b and e) are strongly amplitude-modulated (the origin of which will be explained in Sect. 4.2). It is noted that the oscillations in the two polarization components are out of phase with each other as can be seen by following the dotted guidelines. Hence it is possible that the total pulse energy remains constant despite the apparent redistribution of intensity. Note that these oscillations are not the interference fringes of spectral interferometry. The interference spectra between shaped field and reference field are rather shown in Fig. 7c and f, and the fringe spacing is much narrower than the distance between two intensity peaks of the shaped laser field in Fig. 7b and e. The amplitude modulation shows up in the interference spectra as a beating structure. The data analysis of Fig. 7 by the Fourier-transform method [46, 50, 51] leads to a complete

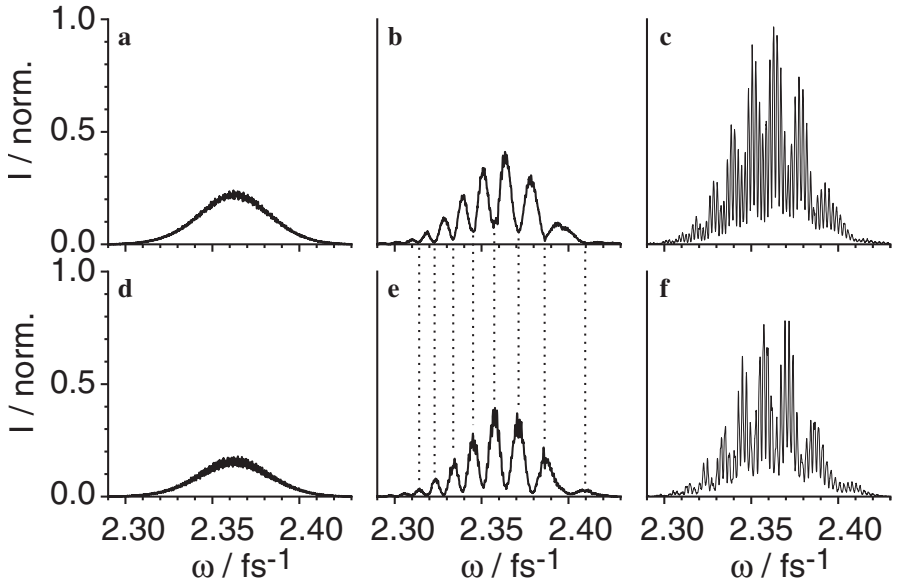

FIGURE 7 Dual-channel spectral interferometry. This graph shows experimental data as follows: **a** component 1 of reference laser field, **b** component 1 of shaped field, **c** component 1 of combined fields, **d** component 2 of reference field, **e** component 2 of shaped field, and **f** component 2 of combined fields. The intensities of the different spectra relative to each other have been preserved in this figure. The *dotted guidelines* emphasize that the intensity modulations in components 1 and 2 are out of phase with each other

characterization of the polarization-shaped laser pulse (see Sect. 4.4).

4.2 *Polarization-state modifications*

It was seen in Fig. 7 that the introduction of spectral phase modulation to the polarization components 1 and 2 led to spectral amplitude modulation in the same components (Fig. 7b and e). The reason for that is based on additional polarization-state modification by the optical elements between the LCD and the location of pulse characterization. It is therefore very important to characterize the pulse shapes directly at the point of the experiment, or to find a way which takes into account additional variations. The Fresnel formulas of classical optics [54] predict that the reflection and transmission properties of optical elements depend on the light polarization with respect to the plane of incidence (with the two principal cases of *s* polarization and *p* polarization). Consider the case where only the amplitudes – and not the phases – of the reflection or transmission coefficients of optical elements are different for the two polarization components E_x and E_y. This situation occurs with the optical gratings inside the zero-dispersion compressor, for example, which have polarization-dependent diffraction efficiencies. In the experimental setup (Fig. 1), compensation for this amplitude modulation is accomplished by the stack of glass plates at Brewster's angle. These glass plates preferentially reflect *x*-polarized light such that the transmitted beam has a reduced amplitude in the *x* component. However, despite the compensation of the amplitude transmission differences, in general the phases of the reflection and transmission coefficients can still be different for *x* and *y* polarization. This has the consequence that pure spectral phase modulation by the LCD along the coordinates E_1 and E_2, followed by pure spectral phase modulation by additional optical elements along the coordinates E_x and E_y, leads to amplitude modulation along the components E_1 and E_2, which depend upon the pulse-shaper settings. This leads exactly to the observation made in connection with the experimental example of Fig. 7b and e that the amplitude modulations for the different spectral regions (i.e. for different LCD phase differences $\Phi_2 - \Phi_1$) are out of phase with each other. The sum of spectral intensities $A_1^2 + A_2^2$ for each spectral component is then independent of the pulse shape. Similar to the Brewster-plate setup for amplitude compensation, it would be possible in principle to compensate for the phase-shifting effects by introduction of suitable wave-plate combinations – if the phase shift is not frequency-dependent.

How can these effects quantitatively be predicted and understood? Of course, one could try to use the Fresnel formulas to calculate the phase and amplitude modulation imposed by each optical surface upon propagation of the laser pulse from the LCD to the experiment. However, there are a number of difficulties associated with this procedure. First, the indices of refraction of the optical elements – which are, furthermore, frequency-dependent in general – would have to be known very accurately. Next, the orientation of some elements with respect to the laboratory-frame coordinate system would be very complicated to be measured exactly. The errors when analyzing an increased number of optical elements all accumulate such that a precise prediction of polarization-shaped laser pulses would not be possible in this way.

4.3 *Experimental Jones-matrix determination*

We have developed a method which takes into account all polarization-state modification effects by suitable experimental calibration employing Jones calculus. This quantitative treatment is described in this section.

In the case of polarization-shaped laser pulses, the electric field can be written as a two-component vector as in (3). Since $E(t)$ is real, knowledge of the positive frequency part is sufficient for a full characterization of the complex-valued spectral light field $E(\omega)$. One therefore defines [47]

$$E^+(\omega) = \begin{cases} E(\omega) & \text{if } \omega \geq 0, \\ 0 & \text{if } \omega < 0. \end{cases} \tag{17}$$

The transfer function of a linear – and not necessarily isotropic – optical element can then be written as a two-by-two complex-valued frequency-dependent matrix [55], called Jones matrix $J(\omega)$, which relates the complex electric output field $\boldsymbol{E}^{+}_{\mathrm{out}}(\omega)$ to the input field $\boldsymbol{E}^{+}_{\mathrm{in}}(\omega)$ by

$$\begin{pmatrix} E^{+}_{1,\mathrm{out}}(\omega) \\ E^{+}_{2,\mathrm{out}}(\omega) \end{pmatrix} = \begin{pmatrix} J_{11}(\omega) J_{12}(\omega) \\ J_{21}(\omega) J_{22}(\omega) \end{pmatrix} \begin{pmatrix} E^{+}_{1,\mathrm{in}}(\omega) \\ E^{+}_{2,\mathrm{in}}(\omega) \end{pmatrix}. \tag{18}$$

If not simply one but n optical components are involved, the total Jones matrix $J(\omega)$ is given by a multiplication of the individual Jones matrices $J^{(i)}(\omega)$:

$$J(\omega) = J^{(n)}(\omega) J^{(n-1)}(\omega) \cdots J^{(1)}(\omega). \tag{19}$$

The action of the polarization pulse shaper can then be described as a product of different Jones matrices, relating the electric input field $\boldsymbol{E}^{+}_{\mathrm{in}}(\omega)$ directly in front of the first beam splitter with the electric output field $\boldsymbol{E}^{+}_{\mathrm{out}}(\omega)$ at the location of the experiment by

$$\begin{pmatrix} E^{+}_{1,\mathrm{out}} \\ E^{+}_{2,\mathrm{out}} \end{pmatrix} = \begin{pmatrix} J^{(2)}_{11} J^{(2)}_{12} \\ J^{(2)}_{21} J^{(2)}_{22} \end{pmatrix} \begin{pmatrix} \mathrm{e}^{\mathrm{i}\Phi_1} & 0 \\ 0 & \mathrm{e}^{\mathrm{i}\Phi_2} \end{pmatrix} \begin{pmatrix} J^{(1)}_{11} J^{(1)}_{12} \\ J^{(1)}_{21} J^{(1)}_{22} \end{pmatrix} \begin{pmatrix} E^{+}_{1,\mathrm{in}} \\ E^{+}_{2,\mathrm{in}} \end{pmatrix}. \tag{20}$$

Here, $J^{(1)}(\omega)$ describes the combined action of all optical elements from the first beam splitter up to the LCD; $\Phi_1(\omega)$ and $\Phi_2(\omega)$ describe the spectral phase modulations imposed by the LCD layers 1 and 2, respectively; and $J^{(2)}(\omega)$ describes how the polarization-shaped laser pulses are then modified by the combination of optical elements between LCD and experiment. If x-polarized input light is used, then of course $E^{+}_{1,\mathrm{in}} = E^{+}_{2,\mathrm{in}}$. It is remarked here that (20) is very general, and that it also accounts for the possibility that the coordinate systems in which the input field, the phase modulation, and the output field are defined are not identical. Coordinate transformations can always be described by additional complex matrices within the Jones products, and hence this description includes the possibility that the LCD or the analyzing polarizer used in the dual-channel spectral interferometry setup are not perfectly aligned along $\pm 45^{\circ}$ with respect to the laboratory-frame x axis.

The goal of the Jones-matrix analysis is to find a relation between the phase modulations $\Phi_1(\omega)$ and $\Phi_2(\omega)$ introduced by the pulse shaper and the electric output laser field $\boldsymbol{E}^{+}_{\mathrm{out}}(\omega)$ at the location of the experiment. As seen from (20), this requires the knowledge of the Jones matrices $J^{(1)}(\omega)$ and $J^{(2)}(\omega)$ as well as the electric input field $\boldsymbol{E}^{+}_{\mathrm{in}}(\omega)$. However, experimental determination of all required parameters is not trivial. Simplification can be achieved by carrying out the matrix multiplication such that (20) can be written as

$$\begin{pmatrix} E^{+}_{1,\mathrm{out}} \\ E^{+}_{2,\mathrm{out}} \end{pmatrix} = \begin{pmatrix} a_{11} & a_{12} \\ a_{21} & a_{22} \end{pmatrix} \begin{pmatrix} \mathrm{e}^{\mathrm{i}\Phi_1} \\ \mathrm{e}^{\mathrm{i}\Phi_2} \end{pmatrix}. \tag{21}$$

Thereby the action of the "passive" optical elements – contained in the two-by-two matrix – can be separated from the action of the "active" LCD – contained in the two-component vector. The "passive" matrix is independent of the applied phase modulations, with the complex matrix parameters a_{kl} containing factors of the input electric fields and the Jones-matrix elements for the same frequency component ω. This a_{kl} matrix is therefore identical for all possible pulse shapes, which forms the basis for its experimental determination. For that purpose, a number of different phase modulations $\Phi_1(\omega)$ and $\Phi_2(\omega)$ are applied and the resulting output laser fields $\boldsymbol{E}^{+}_{\mathrm{out}}(\omega)$ are measured by dual-channel spectral interferometry. If sufficiently many independent pulse shapes are analyzed, the matrix can be determined through (21).

Assume that m different pulse shapes are produced and analyzed. In the set of equations (21) the matrix coefficients a_{kl} are unknown. Since the matrix coefficients are complex and (21) is not written in the standard form of a linear equation system, the matrix multiplication is carried out explicitly for the real and imaginary part of the electric field components. These $4m$ individual relations can be combined into a single real-valued linear equation system, and the unknown parameters a_{kl} can then be determined by a least-squares fit. This fit is performed independently for each spectral component ω that is detected with the multichannel spectrometer. In principle, it is not important which phase shapes are applied in this procedure. However, the phases Φ_1 and Φ_2 in the different measurements should sample a broad distribution of values out of their definition intervals $[-\pi, \pi]$ to keep the experimental uncertainties low. It is important here that the measured relative phase relations between all pulses have to be preserved in the spectral interferometry analysis. Once the parameters of the fit are determined, all possible pulse shapes can be predicted by using (21), and the pulse-shape modifications induced by the optical elements are quantitatively accounted for. Phase stability is then no longer required.

The result of an experimental determination of the coefficients a_{kl} is shown in Fig. 8. The absolute magnitudes of these coefficients (Fig. 8a) contain the spectral amplitudes of the input light. This is reflected by the shape of these distributions. In Fig. 8b it can be seen that the phases of the four coefficients of the a_{kl} matrix are not identical. These mutual phase offsets have the consequence that additional phase modulation occurs in the "passive" optical elements of the polarization pulse shaper, leading to energy transfer between polarization components $E_1(\omega)$ and $E_2(\omega)$ as observed in Fig. 7b and e. The curvatures of the spectral a_{kl} phases indicate the introduction of chirp within the pulse-shaper setup. This can be explained mainly by material dispersion within the stack of Brewster glass plates even if the zero-dispersion setup itself is perfectly aligned. However, this dispersion effect is not critical, because such phase modulations can be compensated for by the pulse shaper itself [10–13]. Note that the ambiguity of an overall frequency-independent phase factor remains in the Jones analysis. This simply reflects the fact that the absolute phase between envelope and carrier wave was not measured. However, this is not a limitation on the characterization method for the pulse durations considered here.

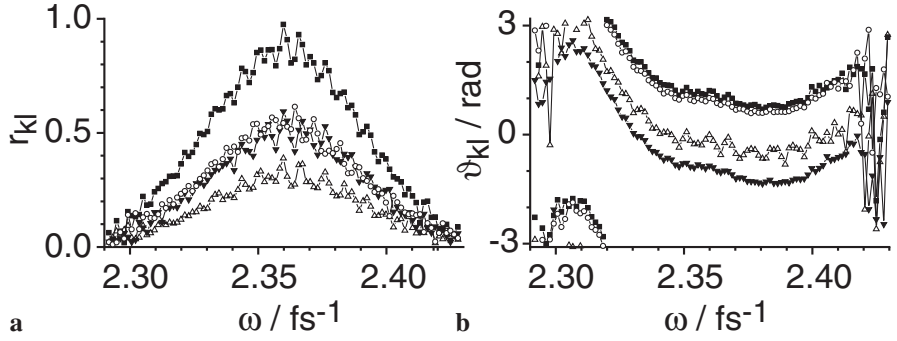

FIGURE 8 Experimental Jones-matrix determination. The results of the least-squares fit are **a** the absolute magnitudes and **b** the phases of the frequency-dependent matrix coefficients a_{11} (*solid squares*), a_{12} (*open circles*), a_{21} (*solid triangles*), and a_{22} (*open triangles*). Not all data points acquired are shown in this figure. The pulse shapes used for this fit were generated by applying the following four pairs of spectrally constant phases: $\{\Phi_1/\text{rad}, \Phi_2/\text{rad}\} = \{b_0 = 3.0, b_0 = 0.0\}$, $\{b_0 = -1.78, b_0 = 0.0\}$, $\{b_0 = 0.0, b_0 = 1.5\}$, and $\{b_0 = 0.0, b_0 = 3.0\}$

4.4 *Comparison of spectral interferometry and Jones calculus*

In this section, a comparison of the polarization pulse characterization methods described in Sect. 4.1 and 4.3 – dual-channel spectral interferometry and Jones calculus – is given in order to demonstrate that they deliver consistent results.

In Fig. 9, the different characterization methods for polarization-shaped laser pulses are compared for a sample pulse. The output of an idealized pulse shaper is shown in Fig. 9a. A perfect Gaussian-shaped input laser spectrum is assumed. Since no additional pulse modification effects are included, the spectra of the two polarization components (top part) are identical and are not amplitude-modulated in any way. The spectral output phases (bottom part) match precisely the LCD-induced phases of $b_1 = 500$ fs for $\Phi_1(\omega)$ (dashed line) and $b_2 = 5 \times 10^3$ fs^2 for $\Phi_2(\omega)$ (solid line). However, it was seen in the previous sections that additional pulse modifications occur in a "real-world" pulse shaper. Experimental characterization of this laser pulse by dual-channel spectral interferometry (obtained by analyzing the spectra of Fig. 7) is shown in Fig. 9b. The spectral intensities here (top part) are identical to those already shown in Fig. 7b and e. The general shapes of the output phases (Fig. 9b, bottom part) are similar to the ideal case, but some distortions are clearly seen. These distortions are due to the "mixing" of polarization components. Using the experimentally determined pulse-shaper matrix of Fig. 8, the output pulse shape can be accurately predicted (Fig. 9c). Comparing Fig. 9b and c, it can be seen that the spectral intensity modulations (top parts) and the phase distortions (bottom parts) are precisely reproduced by Jones calculus. It is thus possible to understand quantitatively the complete behavior of the polarization pulse shaper.

4.5 *Generation of complex experimental pulse shapes*

In the previous example, one could argue that such a laser pulse could also have been produced by "conventional" methods (without a pulse shaper), by interferometric splitting of the two polarization components, introduction of spectral phases with the help of grating compressors, and collinear recombination at the desired temporal delay. Of course, the conventional method would require interferometric stability as well as mechanical reconstruction and extensive alignment each time the pulse parameters would need to be changed.

In the following example, however, a very complex polarization-modulated laser pulse is generated by applying highly-structured spectral phases to both LCD layers, thus demonstrating the full capabilities of the computer-controlled polarization pulse shaper. The resulting pulse is analyzed by dual-channel spectral interferometry (as described in Sect. 4.1), and the elliptical pulse parameters are calculated as functions of time (as described in Sect. 3.1).

The quasi-three-dimensional representation of that light pulse is shown in Fig. 10. Such a laser pulse could simply not

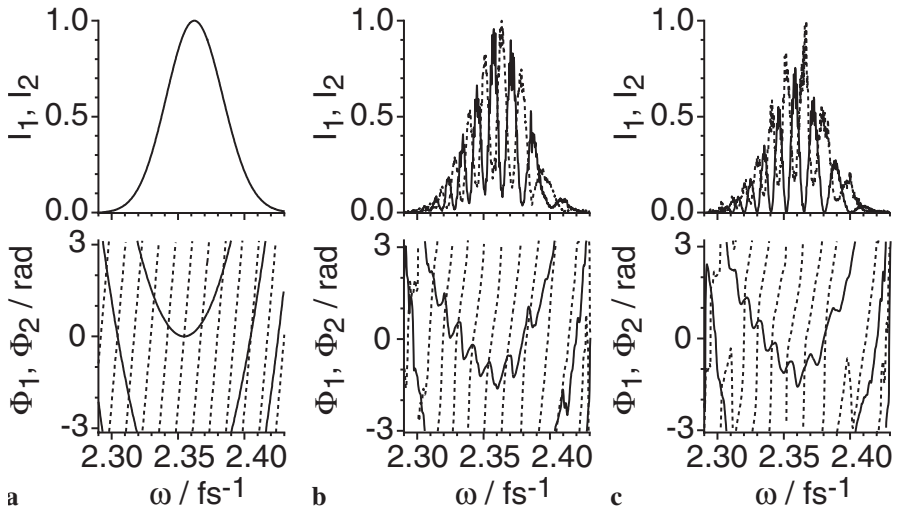

FIGURE 9 Comparison of polarization pulse characterization methods. Spectral intensities (*top row*) and spectral phases (*bottom row*) of a polarization-shaped laser pulse are shown for the polarization components 1 (*dashed lines*) and 2 (*solid lines*) as determined **a** by simulation without additional pulse-shape modification, **b** by dual-channel spectral interferometry, and **c** by Jones calculus

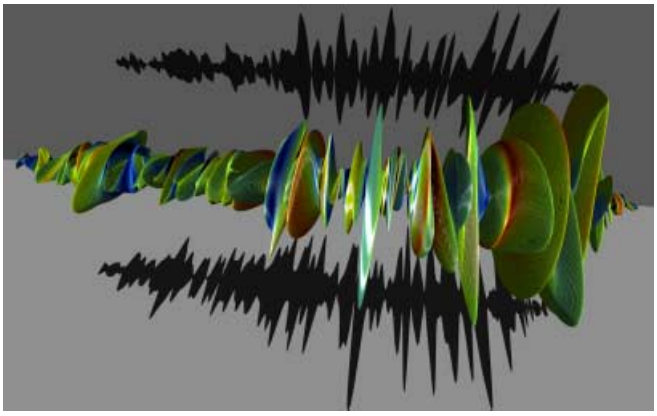

FIGURE 10 Quasi-three-dimensional electric field representation for a complex polarization-modulated laser pulse. Time evolves from left to right, and electric field amplitudes are indicated by the sizes of the corresponding ellipses. The momentary frequency can be indicated by colors, and the shadows represent the amplitude envelopes of component E_1 (*bottom*) and component E_2 (*top*) separately

be produced by any other technique. Note that this pulse is not just a random burst of light but rather a completely coherent and reproducible laser field. The electric field evolves in a highly complex fashion, reaching all kinds of linear, elliptical, and circular polarization with varying orientations of the principal axes as well as varying intensities and oscillation frequencies, within the shown temporal window of 7.5 ps.

5 Conclusion

In this paper, we have described the recently developed [43] technique of computer-controlled femtosecond polarization pulse shaping, where intensity, momentary frequency, and light polarization are varied as functions of time. With the setup shown it is possible to modulate the degree of ellipticity, as well as the orientation of the elliptical principal axes within a single laser pulse, by use of a 128-pixel two-layer LCD inside a zero-dispersion compressor. Two independent and temporally interfering polarization components were treated on an equal footing, reaching equal intensity levels. An immense number of complex pulse shapes can thus be produced. Interferometric stability of the setup is not required because both polarization components travel along an identical beam path.

A mathematical description of these types of laser pulse was developed. It was shown how linear pulse characterization parameters (temporal amplitude envelopes and phase modulations of two orthogonal polarization components) can be transformed into elliptical pulse parameters (total intensity, total phase, ellipticity, and orientation). The desire to combine all four elliptical pulse parameters in a single graph led to quasi-three-dimensional representations which can be understood in an intuitive way. Complete pulse characterization was achieved by implementing dual-channel spectral interferometry so as to be able to characterize the pulse shapes directly at the point of the experiment. As an alternative method, Jones-matrix calculus has been implemented where the frequency-dependent coefficients are determined by an experimental fitting procedure. It is thus possible to understand and quantitatively predict pulse-shape modifications which arise in additional optical elements. The result of the pulse-shape analysis with dual-channel spectral interferometry was then compared with the result from Jones-matrix calculus, showing good agreement.

With the development of femtosecond polarization control, the general prospects for using polarization-shaped light pulses are immense, because the three-dimensional properties of quantum-mechanical wavefunctions can be accessed by controlling the vectorial properties of the electric laser field. Especially for the field of quantum control, the possibility to vary almost arbitrarily the polarization state of light, its intensity and frequency within a single femtosecond laser pulse is of great significance. For the use in adaptive quantum control experiments, we have recently implemented polarization-shaping within a learning loop with an experimental observable as feedback signal [56]. Literally, a new dimension of femtosecond pulse shaping has been opened up.

ACKNOWLEDGEMENTS Financial support from the European Coherent Control Network (COCOMO): HPRN-CT-1999-00129, the German–Israeli Cooperation in Ultrafast Laser Technologies (GILCULT): FKZ-13N7966, and the "Fonds der chemischen Industrie" is gratefully acknowledged.

REFERENCES

1 J.P. Heritage, A.M. Weiner, R.N. Thurston: Opt. Lett. **10**, 609 (1985)
2 A.M. Weiner, J.P. Heritage, E.M. Kirschner: J. Opt. Soc. Am. B **5**, 1563 (1988)
3 A.M. Weiner, D.E. Leaird: Opt. Lett. **15**, 51 (1990)
4 A.M. Weiner, D.E. Leaird, A. Patel, J.R. Wullert II: IEEE J. Quantum Electron. **QE-28**, 908 (1992)
5 M.M. Wefers, K.A. Nelson: Opt. Lett. **20**, 1047 (1995)
6 M.E. Fermann, V. da Silva, D.A. Smith, Y. Silberberg, A.M. Weiner: Opt. Lett. **18**, 1505 (1993)
7 C.W. Hillegas, J.X. Tull, D. Goswami, D. Strickland, W.S. Warren: Opt. Lett. **19**, 737 (1994)
8 E. Zeek, K. Maginnis, S. Backus, U. Russek, M.M. Murnane, G. Mourou, H.C. Kapteyn, G. Vdovin: Opt. Lett. **24**, 493 (1999)
9 A.M. Weiner: Rev. Sci. Instrum. **71**, 1929 (2000)
10 D. Yelin, D. Meshulach, Y. Silberberg: Opt. Lett. **22**, 1793 (1997)
11 T. Baumert, T. Brixner, V. Seyfried, M. Strehle, G. Gerber: Appl. Phys. B **65**, 779 (1997)
12 A. Efimov, M.D. Moores, N.M. Beach, J.L. Krause, D.H. Reitze: Opt. Lett. **23**, 1915 (1998)
13 T. Brixner, M. Strehle, G. Gerber: Appl. Phys. B **68**, 281 (1999)
14 A.M. Weiner, A.M. Kan'an: IEEE J. Sel. Top. Quantum Electron. **4**, 317 (1998)
15 W.S. Warren, H. Rabitz, M. Dahleh: Science **259**, 1581 (1993)
16 S.A. Rice, M. Zhao: *Optical Control of Molecular Dynamics* (Wiley, New York 2000)
17 C.J. Bardeen, V.V. Yakovlev, K.R. Wilson, S.D. Carpenter, P.M. Weber, W.S. Warren: Chem. Phys. Lett. **280**, 151 (1997)
18 A. Assion, T. Baumert, M. Bergt, T. Brixner, B. Kiefer, V. Seyfried, M. Strehle, G. Gerber: Science **282**, 919 (1998)
19 D. Meshulach, Y. Silberberg: Nature **396**, 239 (1998)
20 T. Hornung, R. Meier, D. Zeidler, K.L. Kompa, D. Proch, M. Motzkus: Appl. Phys. B **71**, 277 (2000)
21 T.C. Weinacht, J. Ahn, P.H. Bucksbaum: Nature **397**, 233 (1999)
22 T.C. Weinacht, J.L. White, P.H. Bucksbaum: J. Phys. Chem. A **103**, 10166 (1999)
23 T. Hornung, R. Meier, M. Motzkus: Chem. Phys. Lett. **326**, 445 (2000)
24 T. Hornung, R. Meier, R de Vivie-Riedle, M. Motzkus: Chem. Phys. **267**, 261 (2001)
25 J. Kunde, B. Baumann, S. Arlt, F. Morier-Genoud, U. Siegner, U. Keller: Appl. Phys. Lett. **77**, 924 (2000)
26 R. Bartels, S. Backus, E. Zeek, L. Misoguti, G. Vdovin, I.P. Christov, M.M. Murnane, H.C. Kapteyn: Nature **406**, 164 (2000)
27 P.B. Corkum, N.H. Burnett, M.Y. Ivanov: Opt. Lett. **19**, 1870 (1994)

28 M.Y. Ivanov, P.B. Corkum, T. Zuo, A.D. Bandrauk: Phys. Rev. Lett. **74**, 2933 (1995)
29 E. Constant, V.D. Taranukhin, A. Stolow, P.B. Corkum: Phys. Rev. A **56**, 3870 (1997)
30 M.M. Wefers, H. Kawashima, K.A. Nelson: J. Chem. Phys. **108**, 10248 (1998)
31 M. Shapiro, P. Brumer: J. Chem. Phys. **95**, 8658 (1991)
32 Y. Fujimura, L. Gonzalez, K. Hoki, J. Manz, Y. Ohtsuki: Chem. Phys. Lett. **306**, 1 (1999)
33 M. Shapiro, E. Frishman, P. Brumer: Phys. Rev. Lett. **84**, 1669 (2000)
34 L. Gonzalez, D. Kröner, I.R. Sola: J. Chem. Phys. **115**, 2519 (2001)
35 K. Hoki, Y. Ohtsuki, Y. Fujimura: J. Chem. Phys. **114**, 1575 (2001)
36 K. Hoki, D. Kröner, J. Manz: Chem. Phys. **267**, 59 (2001)
37 W.J. Walecki, D.N. Fittinghoff, A.L. Smirl, R. Trebino: Opt. Lett. **22**, 81 (1997)
38 C. Altucci, C. Delfin, L. Roos, M.B. Gaarde, A. L'Huillier, I. Mercer, T. Starczewski, C.-G. Wahlström: Phys. Rev. A **58**, 3934 (1998)
39 M. Kakehata, R. Ueda, H. Takada, K. Torizuka, M. Obara: Appl. Phys. B **70**, S207 (2000)
40 D.N. Villeneuve, S.A. Aseyev, P. Dietrich, M. Spanner, M.Yu. Ivanov, P.B. Corkum: Phys. Rev. Lett. **85**, 542 (2000)
41 Z.Z. Zhuang, S.W. Suh, J.S. Patel: Opt. Lett. **24**, 694 (1999)
42 R.L. Eriksen, P.C. Mogensen, J. Glückstad: Opt. Commun. **187**, 325 (2001)
43 T. Brixner, G. Gerber: Opt. Lett. **26**, 557 (2001)
44 C. Froehly, A. Lacourt, J.C. Vienot: J. Opt. (Paris) **4**, 183 (1973)
45 J. Piasecki, B. Colombeau, M. Vampouille, C. Froehly, J.A. Arnaud: Appl. Opt. **19**, 3749 (1980)
46 L. Lepetit, G. Cheriaux, M. Joffre: J. Opt. Soc. Am. B **12**, 2467 (1995)
47 J.-C. Diels, W. Rudolph: *Ultrashort Laser Pulse Phenomena* (Academic Press, London 1996)
48 D.J. Kane, R. Trebino: IEEE J. Quantum Electron. **QE**-**29**, 571 (1993)
49 R. Trebino, K.W. DeLong, D.N. Fittinghoff, J.N. Sweetser, M.A. Krumbügel, B.A. Richman, D.J. Kane: Rev. Sci. Instrum. **68**, 3277 (1997)
50 C. Dorrer, N. Belabas, J.P. Likforman, M. Joffre: J. Opt. Soc. Am. B **17**, 1795 (2000)
51 C. Dorrer, N. Belabas, J.P. Likforman, L. Joffre: Appl. Phys. B **70**, S99 (2000)
52 D.N. Fittinghoff, J.L. Bowie, J.N. Sweetser, R.T. Jennings, M.A. Krumbügel, K.W. DeLong, R. Trebino, I.A. Walmsley: Opt. Lett. **21**, 884 (1996)
53 O. Buccafusca, X. Chen, W.J. Walecki, A.L. Smirl: J. Opt. Soc. Am. A **15**, 1218 (1998)
54 M.V. Klein, T.E. Furtak: *Optics*, 2nd edn. (Wiley, New York 1986)
55 A. Gerrard, J.M. Burch: *Introduction to Matrix Methods in Optics* (Wiley, New York 1975)
56 T. Brixner, N.H. Damrauer, G. Krampert, P. Niklaus, G. Gerber: to be published